AGU PUBLICATIONS

JGR

Journal of Geophysical Research: Biogeosciences

RESEARCH ARTICLE
10.1002/2013JG002489

Key Points:
- Landsat imagery was used to assess aspen forest recovery due to recent drought
- Brightness but not vegetation cover has returned to predrought conditions
- Die-off reduced the canopy cooling effect and elevated surface temperature

Correspondence to:
C.-y. Huang,
choying@ntu.edu.tw

Citation:
Huang, C.-y., and W. R. L. Anderegg (2014), Vegetation, land surface brightness, and temperature dynamics after aspen forest die-off, *J. Geophys. Res. Biogeosci.*, *119*, 1297–1308, doi:10.1002/2013JG002489.

Received 20 AUG 2013
Accepted 6 JUN 2014
Accepted article online 13 JUN 2014
Published online 15 JUL 2014

Vegetation, land surface brightness, and temperature dynamics after aspen forest die-off

Cho-ying Huang[1] and William R. L. Anderegg[2]

[1]Department of Geography, National Taiwan University, Taipei, Taiwan, [2]Princeton Environmental Institute, Princeton University, Princeton, New Jersey, USA

Abstract Forest dynamics following drought-induced tree mortality can affect regional climate through biophysical surface properties. These dynamics have not been well quantified, particularly at the regional scale, and are a large uncertainty in ecosystem-climate feedback. We investigated regional biophysical characteristics through time (1995–2011) in drought-impacted (2001–2003), trembling aspen (*Populus tremuloides* Michx.) forests by utilizing Landsat time series green and brown vegetation cover, surface brightness (total shortwave albedo), and daytime land surface temperature. We quantified the temporal dynamics and postdrought recovery of these characteristics for aspen forests experiencing severe drought-induced mortality in the San Juan National Forest in southwestern Colorado, USA. We partitioned forests into three categories from healthy to severe mortality (Healthy, Intermediate, and Die-off) by referring to field observations of aspen canopy mortality and live aboveground biomass losses. The vegetation cover of die-off areas in 2011 (26.9% of the aspen forest) was significantly different compared to predrought conditions (decrease of 7.4% of the green vegetation cover and increase of 12.1% of the brown vegetation cover compared to 1999). The surface brightness of the study region 9 years after drought however was comparable to predrought estimates (12.7–13.7%). Postdrought brightness was potentially influenced by understory shrubs, since they became the top layer green canopies in disturbed sites from a satellite's point of view. Satellite evidence also showed that the differences of land surface temperature among the three groups increased substantially (≥45%) after drought, possibly due to the reduction of plant evapotranspiration in the Intermediate and Die-off sites. Our results suggest that the mortality-affected systems have not recovered in terms of the surface biophysical properties. We also find that the temporal dynamics of vegetation cover holds great potential for assessing propensity of subsequent mortality during drought itself, which could provide effective monitoring and potentially a much needed "early warning" of drought-induced tree mortality.

1. Introduction

Large-scale tree die-off events have been highlighted as a major disturbance in forests across a broad spectrum of biomes in the last decade [*van Mantgem et al.*, 2009; *Allen et al.*, 2010]. While the factors that triggered die-off in forests around the world are complicated and likely differ from region to region, many tree mortality events have been attributed to a combined driver of prolonged drought with elevated temperature concomitant with or followed by insect and pathogen outbreaks [*McDowell et al.*, 2011]. These forest mortality events can have a major influence on the regional and continental biogeochemical, hydrological, and energy cycles [*Anderegg et al.*, 2012a].

Recent studies have examined the ramifications of widespread tree mortality on forest carbon cycles [*Kurz et al.*, 2008; *Huang et al.*, 2010; *Hicke et al.*, 2012] and started to assess the changes to energy budgets [*Royer et al.*, 2011]. Forest energy budgets are strongly influenced by land surface properties such as vegetation cover (defined as the percentage of ground surface covered when viewing planometrically from the top) of photosynthetically active vegetation (or "green vegetation cover" hereafter) and nonphotosynthetically active vegetation (e.g., bark, coarse woody debris, and snags, hereafter "brown vegetation cover") and surface brightness (total shortwave albedo subsequently used interchangeably). These land surface properties could also influence land surface temperature substantially [*Anderson et al.*, 2011]. Thus, remote sensing techniques that quantify the dynamics of these parameters during widespread tree mortality over a vast region could greatly improve our understanding of the tree mortality's role in ecosystem functioning, as well as biophysical and biogeochemical feedback, to shifts in climate [*Bonan*, 2008]. In addition, these techniques could also enable near-real-time monitoring of vegetation dynamics, holding the potential to provide "early warning" signs of

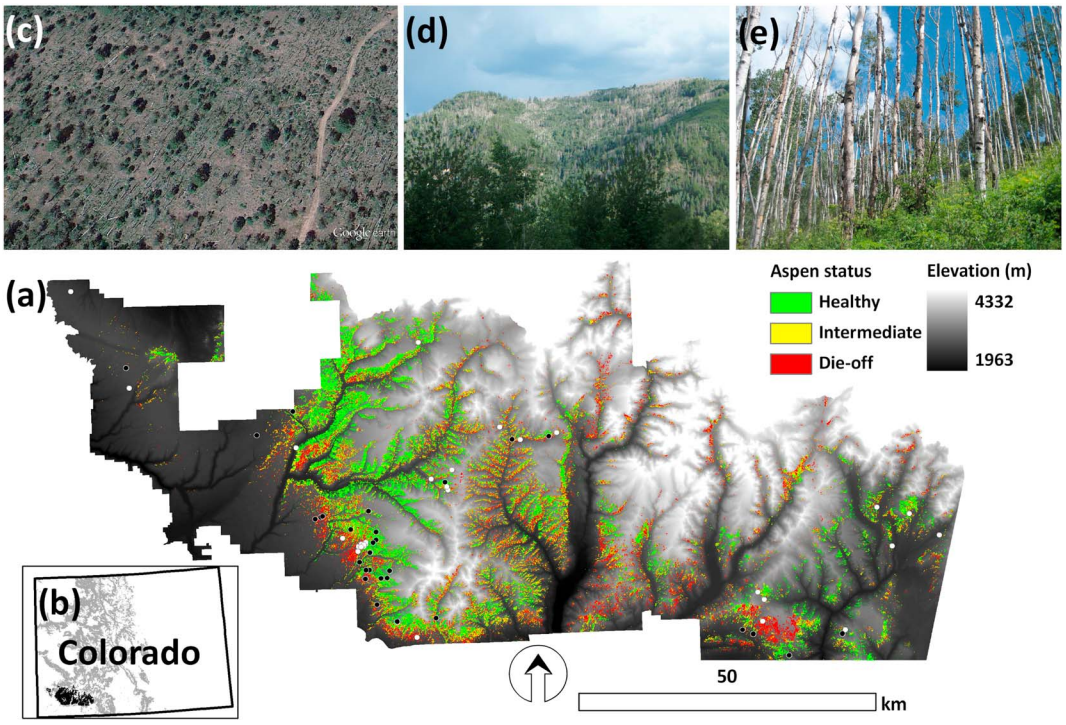

Figure 1. (a) The study region: Aspen forests in the San Juan National Forest covered by the Landsat Worldwide Reference System–path 35, row 34. The top layer depicts aspen health status (see Table 1 for details), and the background is a 30 m spatial resolution digital elevation model. Widely distributed circles ($n = 60$) are the field sites, and black circles ($n = 30$) are ones with leaf area index measures. (b) The location of study site (black pixels) and distribution of aspen forests (gray pixels) in Colorado. Photographic illustrations of aspen die-off are shown from (c) a high-resolution satellite image (Google Earth, the site visited and confirmed in summer 2011) and as (d) a landscape view and (e) a close-up look. The image date was 8 August 2011, and the photographs were taken by W. Anderegg in summer 2010.

ongoing or incipient tree mortality if physiological responses such as leaf shedding, decrease in leaf area index (LAI), or branch die-off can be detected via remote sensing.

Trembling aspen (*Populus tremuloides* Michx., hereafter "aspen") forests have experienced a recent and severe die-off in many parts of western North America such as Aspen Parkland, Kapuskasing (Canada), northern Lake States, and southern Rocky Mountains (U.S.) (for a comprehensive description see, *Worrall et al.* [2013]). This clonal tree is considered the most widely spread tree species in the continent [*Mitton and Grant*, 1996]. First reported in 2004, the damage from aspen die-off expanded exponentially in Colorado through 2008 and has since slowed or stabilized according to aerial survey data [*Worrall et al.*, 2010]. Research on aspen decline is relatively sparse compared to tree die-off in other vegetation types. Most research to date has investigated the climatic factors and related biotic agents [*Hanna and Kulakowski*, 2012; *Worrall et al.*, 2013] that induced aspen die-off, the impacts of it on green vegetation cover, carbon storage and productivity [*Hogg et al.*, 2008; *Huang and Anderegg*, 2012], and the physiological mechanisms underlying aspen die-off [*Anderegg et al.*, 2012b, 2013]. However, little research has addressed the predrought and postdrought dynamics and recovery of major land biophysical characteristics, such as vegetation cover, surface brightness, and land surface temperature, which are important in biogeochemical, hydrological, and energy cycles [*Anderson et al.*, 2011]. In this study, we derive the aforementioned land surface parameters from time series remotely sensed images to investigate the recovery of aspen forests at the regional scale. We further examine detectable changes during drought itself (but before significant tree mortality) that could provide near-real-time monitoring and early warning signals of impending forest die-off.

2. Methods

2.1. Site Description

We focused on the aspen forests in the San Juan National Forest located in southwestern Colorado, USA (Figure 1) at midaltitude (2350–3250 m above sea level). The region was delineated by referring to a

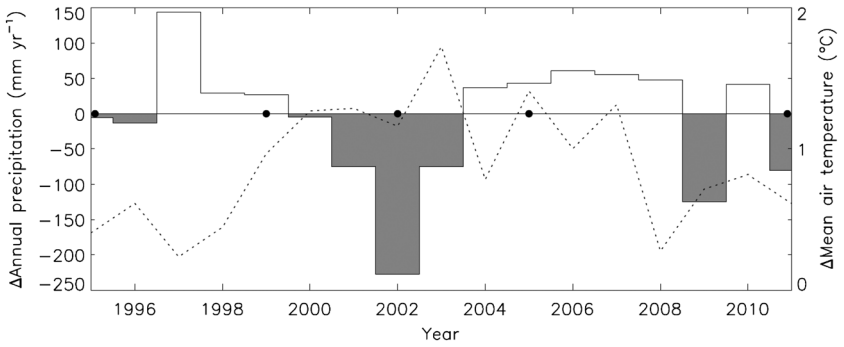

Figure 2. Differences (Δ) of annual precipitation (white bar: above long-term average and gray bar: below average) and mean air temperature (dashed line) to the long-term (1895–2011) averages (mean annual precipitation = 699.7 mm yr^{-1} and mean air temperature = 3.9°C) of the study region during the observation period (1995–2011) using the Parameter-elevation Regressions on Independent Slopes Model (PRISM) climate data. Black circles indicate the years with the availability of early summer Landsat images for this study.

vegetation map produced by the Southwest Regional Gap Analysis Project [*Lowry et al*., 2007]. In order to match with available remote sensing images, we selected only the area covered by the Landsat Worldwide Reference System–path 35, row 34, comprising about 950 km^2. This mountainous region experiences a summer rainy season that usually begins in July due to an influx of monsoonal air from the Gulf of Mexico and the Gulf of California. Winter storms typically cover higher elevations in snow in mid-November and generally cease in early May [*Keen*, 1996]. The mean annual precipitation and air temperature of the site are 699.7 mm yr^{-1} and 3.9°C, respectively, according to the long-term (1895–2011) averages of the Parameter-elevation Regressions on Independent Slopes Model (PRISM) climate data (http://www.prism.oregonstate.edu/). The dominant understory species is the mountain snowberry (*Symphocarpus oreophilus* A. Gray) (Figure 1e). Prolonged drought (here defined as at least 75 mm yr^{-1} below the long-term mean annual precipitation) lasted for 2 years (2001–2003) (Figure 2), accompanied by elevated summer temperatures, and likely triggered aspen die-off [*Worrall et al*., 2008, 2010]. Recent studies has suggested that aspen die-off in this region was potentially one of the most severe levels of aboveground biomass loss measured in North American forests to date; the mean live aboveground biomass losses reached ≥60 Mg ha^{-1} based upon remote sensing [*Huang and Anderegg*, 2012] and field [*Anderegg et al*., 2012b] estimations.

2.2. Field Observations

Surveys to assess damages of aspen die-off were conducted in summers (June–August) of 2009–2011 by measuring canopy mortality and effective leaf area index (LAI) (defined as the total one-sided area of plant tissue per unit ground surface area [*Bréda*, 2003] multiplied by a foliage clumping index [*Ryu et al*., 2010]). A total of 60 plots were randomly located within the aspen stands, each plot composing one or four 6.3–8 m radius circles with sizes ranging from 0.008 to 0.05 ha. To ensure that plots were not located within the same aspen clone, we observed patterns and timing of leaf flush during late spring to define clonal boundaries. We assessed canopy mortality (%) visually for all aspen trees and excluded snags, fallen logs, and any other tree species within the plots (which were few, as most forests were monospecific). Canopy mortality is defined as abnormal and recent senescence of branches and twigs within the tree crown at the stand level. Percent canopy mortality was assessed across plots by two observers for consistency, which was generally high (±3.7% standard deviation (sd)). The approach has been applied successfully in other aspen die-off studies, and the estimates generally correlate well ($r = -0.96$, $n = 30$ stands) with changes in canopy closure assessed with hemispherical (fisheye) photography [*Worrall et al*., 2010; *Anderegg et al*., 2012b].

Canopy gap fraction (the fraction of view unobstructed by canopy in any particular direction [*Welles and Cohen*, 1996]) of 30 plots (Figure 1a) across a gradient of canopy mortality severity was measured by fisheye photography in the summer of 2009 ($n = 22$) and 2011 ($n = 8$). The photographs were taken at 2 m height above understory shrubs at the plot center during the predawn period before sunrise (typically 0500–0600 h) using automatic exposure settings and oriented with respect to north with a compass. The effective LAI for each plot/stand was calculated through gap fraction from each photograph using the

Gap Light Analyzer program (Simon Fraser University, BC, Canada and Cary Institute of Ecosystem Studies, NY, USA). Since the complexity of mountainous terrain of the study region and dense understory vegetation in the aspen forests (Figure 1e) might be present in the border of a fisheye photograph and result in the overestimation [*Jelaska et al*., 2006], a narrow zenith angle of 0°–60° was selected to integrate the effective LAI.

2.3. Satellite Vegetation Cover Fractions

Four sets of early summer Landsat Thematic Mapper (TM), 5 May 1995, 30 June 1999, 30 June 2005, and 1 July 2011 and a set of Enhanced Thematic Mapper plus (ETM+, 30 June 2002) for the Landsat Worldwide Reference System–path 35, row 34 with cloud cover ≤5%, were acquired from the U.S. Geological Survey (http://glovis.usgs.gov). Image acquisition dates are controlled within 6 days to minimize unrelated potential uncertainties such as sensor-Sun geometrical and phenological changes. The image acquired in 1999 presents the predrought baseline condition, since it was right before the onset of the consecutive years of severe drought (Figure 2). We confirmed it by comparing the land surface characteristics (green and brown vegetation cover, total shortwave albedo, and land surface temperature) with those derived from the 1995 image, since both years yielded similar annual precipitation and mean air temperature (Figure 2). Images collected in 2002, 2005, and 2011 depict the driest period, the transition stage, and the current condition, respectively. Landsat TM and ETM+ are multispectral spaceborne sensors containing six optical bands with a nominal spatial resolution of 30 m and one thermal band (pixel size = 120 m for TM and 60 m for ETM+). The images were georegistered by the U.S. Geological Survey prior to the acquisition in the Universal Transverse Mercator zone 12 N and the datum of the World Geodetic System 1984. For atmospheric correction, the image was converted from 8 bit raw digital count to surface reflectance using ACORN version 6 (ImSpec LLC, CA, USA). Two atmospheric parameters are required for the Landsat mode: atmospheric water vapor and atmosphere visibility. The assumption of similar atmospheric conditions among images was made since all images were acquired under good weather conditions, with no or very limited amount of cloud cover, and were acquired in the same season. They were set to 15 mm (atmospheric water vapor) and 100 km (atmosphere visibility) by referring to the user manual [*ACORN*, 2008].

Spectral mixture analysis is a technique to derive subpixel cover fractions of surface materials collected from remotely sensed data. In a natural setting, the main surface components (also known as end-members) are green (GV) and brown (BV) vegetation cover and bare soil. Each end-member component contributes to the pixel-level spectral reflectance (ρ_{pixel}) as the linear combination of end-member (e) spectra:

$$\begin{aligned} \rho_{pixel} &= \Sigma[\rho_e \cdot C_e] + \varepsilon \\ &= [\rho_{GV} \cdot C_{GV} + \rho_{BV} \cdot C_{BV} + \rho_{soil} \cdot C_{soil}] + \varepsilon \end{aligned} \tag{1}$$

$$\Sigma[C_e] = 1.0 \tag{2}$$

where C is the cover fraction of each end-member and ε is the error term (equation (1)), and the summation of the end-member fractions equates to unity (equation (2)). There are algorithms to take natural variability of end-members into account by random selection of end-members from spectral libraries (or bundles [*Bateson et al*., 2000]) based upon a Monte Carlo simulation (for details, see *Asner and Lobell* [2000]). The model is very robust and has been applied in many different kinds of vegetation types (drylands, rainforests, etc.) with high estimation accuracy (85–95%) [*Asner et al*., 2009]. We constructed end-member bundles for green ($n = 83$, aspen canopies and other dominant woody and herbaceous species) and brown ($n = 51$, snags and ground litters) vegetation cover and bare soil ($n = 40$) acquired from the same bioclimatic regions by a full optical range (350–2500 nm), 1 nm resolution spectroradiometer (Analytical Spectral Devices, Inc., CO, USA) (data sources: the National Biological Information Infrastructure [http://frames.nbii.gov], U.S. Geological Survey Digital Spectral Library [http://speclab.cr.usgs.gov], and Drought Impacts on Regional Ecosystems Network [http://www4.nau.edu/direnet/index.html]). The green and brown vegetation cover was collected at the canopy scale, and all data contained shadow fractions. The data were convoluted to six multispectral bands in order to match up with the Landsat TM or ETM+ spectral profiles. The spectral characteristics and specific setup for the spectral mixture analysis can be found in *Huang and Anderegg* [2012]. Healthy aspen forests contain high canopy closure, and very dense understory shrub cover is commonly present (Figure 1e). Therefore, bare soil is often negligible from the satellite view even in an aspen die-off site, and only green and brown vegetation cover fractions were selected for the analysis.

2.4. Satellite Vegetation Cover Association

Previous studies have demonstrated that the end-member fractions can be treated as surrogates for ground-measured-projected cover types and have been validated in semiarid environments, where the statures of trees and shrubs are low [*Harris et al*., 2003; *Huang et al*., 2009]. It is extremely difficult to validate the satellite estimates of green and brown vegetation cover in aspen forests where tree height is generally above 15 m. In some cases, submeter, high spatial resolution satellite images can be used to delineate land surface characteristics as an alternative approach when the position of observation is hard to reach. However, due to the high level of mixture of green and brown canopies of the region, it is not feasible even using the finest-resolution satellite image (ground sample distance ≤ 50 cm). Thus, in this study, we assumed that observations from the ground (below canopy) should be relatively similar to those measured from the top of canopy, which is viewed by a satellite sensor. Our aims here were to assess the temporal dynamics and postdrought recovery (relative changes of the same pixels over time, rather than absolute values) at a regional scale and to evaluate the ecological relevance of remotely sensed metrics. Therefore, we correlated remotely sensed green and brown vegetation cover data with ground-measured overstory LAI (greenness) and canopy mortality (exposed branches) [*Huang and Anderegg*, 2012], respectively, using both parametric (the Pearson product moment correlation coefficient (r)) and nonparametric (the Theil–Sen estimator) approaches (JMP v. 11, SAS Institute Inc., NC, USA and R zyp package, http://www.r-project.org/). The Theil−Sen estimator is a robust linear regression for estimating a linear trend of a set of data that are insensitive to outliers [*Fernandes and Leblanc*, 2005]. The analysis is not meant to upscale LAI and canopy mortality to the landscape scale but instead to connect satellite metrics with ecologically relevant field-measured vegetation parameters.

2.5. Remotely Sensed Brightness and Land Surface Temperature Data

Brightness (total shortwave albedo [ρ_{short}]) is a pivotal parameter for affecting terrestrial energy budgets [*Anderson et al*., 2011], which can be computed using the following linear regression model (equation (3) [*Liang*, 2000]):

$$\rho_{\text{short}} = 0.356\rho_1 + 0.130\rho_3 + 0.373\rho_4 + 0.085\rho_5 + 0.072\rho_7 - 0.0018 \tag{3}$$

where the subscripts indicate the band numbers of a Landsat TM or ETM+ image. We multiplied this proportion by 100 to present values as percentage (%) for consistency with the green and brown vegetation cover fractions. The temporal dynamics of predrought and postdrought surface brightness data were generated using these five sets of Landsat images.

The daytime (~10:30 A.M. local time) land surface temperature (hereafter "land surface temperature" for simplicity) can be retrieved from Landsat thermal band 6 (10.4–12.5 μm):

$$T = \frac{K_2}{\ln\left(\frac{K_1}{L} + 1\right)} \tag{4}$$

where T is the temperature (K) and L is the radiance ($\text{W m}^{-2}\,\mu\text{m}^{-1}\,\text{sr}^{-1}$). The coefficients K_1 are 607.76 and 666.09, and K_2 are 1260.56 and 1282.71 for TM and ETM+, respectively. A constant band average atmospheric transmission of 0.95 is usually applied to modify K_1 when using atmospherically uncorrected radiance data for ground temperature estimation (http://atmcorr.gsfc.nasa.gov).

2.6. Aspen Forest Classification

To facilitate the analysis and data interpretation, we categorized Landsat-derived contemporary vegetation cover and surface brightness spatial data into three groups: Healthy, Intermediate, and Die-off (Figure 1a). The partition was based upon the current (2009–2011) canopy mortality (Figure 3, photograph insets) and live aboveground biomass loss distributions from field plots in the study site (Figure 1a). The characteristics of aspen structures for each group are summarized in Figure 3 and Table 1. The sample sizes of the three groups generally reflect the landscape-level frequencies according to our field observations. We present a brief description of field aspen live aboveground biomass loss measurements, but for further details, see *Huang and Anderegg* [2012].

To assess live aboveground biomass losses, we measured the diameter at breast height (DBH, defined as stem diameter 1.37 m above the forest floor) for every ramet (an individual plant grows as a clone from

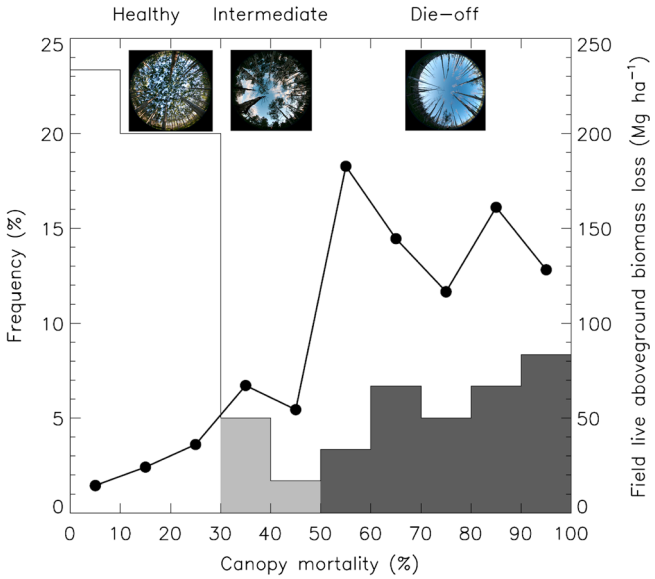

Figure 3. Categories of aspen health groups (Healthy, Intermediate, and Die-off) via frequencies (bars, the left *y* axis) of field aspen canopy mortality observations ($n = 60$) and mean live aboveground biomass losses of each interval (black dots, the secondary *y* axis). Colors of the bars from light to dark indicate the severity of tree mortality. Three insets are fisheye photographs illustrating different stages of canopy mortality from Healthy to Die-off taken by W. Anderegg in summer 2009.

another individual) with a DBH > 5 cm within a plot and converted it to aboveground biomass using a general aspen allometry [*Pastor et al.*, 1984], previously validated for this region by *Huang and Anderegg* [2012]. The live aboveground biomass loss for each tree was estimated by multiplying aboveground biomass by percent canopy mortality, since *Gower et al.* [1997] found a significant positive relationship between leaf area (canopy closure, related to canopy mortality) and DBH (the predictor for aboveground biomass) in aspen forests. The loss of live aboveground biomass density (Mg ha^{-1}) of each plot was estimated by standardizing for plot size.

According to our field observations of aspen mortality, there was a strong correlation between aspen live aboveground biomass losses (y, Mg ha^{-1}) and canopy mortality at the plot scale (x, %; for detailed information and statistics, see Results section):

$$y = 1.59x, \qquad R^2 = 0.79 \tag{5}$$

By referring to Table 1 and equation (5), we can define the range of live aboveground biomass losses to each group. *Huang and Anderegg* [2012] produced a contemporary aspen live aboveground biomass loss map at the continuous scale (unit: Mg ha^{-1}) for the study site using the 1 July 2011 Landsat TM image. Therefore, each pixel in the current study can then be assigned to one of the three groups (Healthy, Intermediate, and Die-off; Figure 1a) according to the group ranges.

2.7. Statistical Analysis

Remotely sensed data usually generates a tremendous amount of data points (in our case more than 1 million pixels), which present challenges for standard statistical tests. The statistical tests of the differences of green and brown vegetation cover and the brightness among aspen health categories are not generally meaningful after taking the sample size into account. In addition, autocorrelation of these spatial data may limit the application of standard statistics [*Isaaks and Srivastava*, 1989]. Therefore, we sampled the data in a random fashion; a simple model (equation (6)) by *Yamane* [1967] was utilized to select a proper sample size:

$$n = N \,/\, \left(1 + N \times \sigma^2\right) \tag{6}$$

Table 1. Description of Three Distinct Groups With Different Degrees of Canopy Mortality[a]

	Plot Scale ($n_{(\text{Healthy})} = 38$, $n_{(\text{Intermediate})} = 4$, $n_{(\text{Die-off})} = 18$)		Landscape Scale
Type (% Canopy Mortality)	Density (Trees ha^{-1}, ±sd)	DBH (cm, ±sd)	Proportion (%)
Healthy (0–30)	1186.1 ± 611.3	22.0 ± 5.9	42.1
Intermediate (31–50)	988.0 ± 217.9	22.4 ± 8.2	31.0
Die-off (51–100)	956.6 ± 438.9	23.2 ± 4.5	26.9

[a]DBH and sd are short for diameter at breast height and standard deviation, respectively.

Figure 4. Strong ($p \le 0.001$ from parametric/nonparametric statistics) positive linear correlations (solid lines) between ground-measured effective (a) LAI (leaf area index, m^2 m^{-2}) and (c) canopy mortality (%) and satellite green and brown vegetation cover fractions (%), respectively. (b) A site photograph of the outlier (the black dots in Figures 4a and 4c) taken by W. Anderegg in summer 2009. The site suffered severe aspen canopy mortality (93.5% loss) with fallen logs and is dominated by lush low stature shrubs mainly mountain snowberry (*Symphoricarpus oreophilus*).

where n, N, and σ are the sample size, the population size, and the uncertainty, respectively. In this study, $\sigma = 0.05$ was assigned.

To investigate the recovery of vegetation cover and surface brightness, we compared these parameters derived from the Landsat images acquired in 1999 (predrought baseline) and 2011 (contemporary condition) of the Healthy, Intermediate, and Die-off groups using one-way analysis of variance (ANOVA). We also conducted the Tukey–Kramer multiple comparison procedure [*Ramsey and Schafer*, 1997], which is a multicomparison model, to test the differences among the three defined groups of the same year. A strict significance level of difference (α) between each class was set to 0.01. Unlike vegetation cover and surface brightness, land surface temperature fluctuates highly and is sensitive to meteorological variation. In addition, there is a direct link between land surface temperature and topography, and previous studies have shown that there were distinct spatial patterns of aspen die-off in the study region [*Worrall et al.*, 2008; *Huang and Anderegg*, 2012]. Therefore, we compared the mean differences (Δ) among the three groups (Die-off versus Healthy, Die-off versus Intermediate, and Intermediate versus Healthy) through time rather than absolute temperature values.

3. Results

3.1. Field Canopy Cover and Validation

The drought-induced canopy mortality of 1736 ramets was assessed from 60 plots. The mean density (±sd) of the plots was 1104.1 ± 551.5 ramets ha^{-1} ranging from 481.2 to 3133.4 ramets ha^{-1}. Our field observations revealed that 30% of the plots experienced significant canopy mortality (>50%), and the mean (±sd) level of mortality was 35.0 ± 31.0%. Variation of ground-measured effective LAI ($n = 30$) was pronounced (0.64 m^2 m^{-2}) with mean, minimum, and maximum of 1.29, 0.12, and 2.56, respectively.

There was a significant positive correlation ($r = 0.56$, $p = 0.001$, and $n = 30$) between field effective LAI and green vegetation cover derived from the 2011 TM image (Figure 4a), which included an apparent outlier (the black dot in Figure 4a). Our effective LAI measurements could potentially underestimate true LAI due to processing methods [*Zhang et al.*, 2005], but the significant positive correlation should not be affected. Investigation of this outlier revealed that top layer aspen trees were severely damaged (93.5% canopy mortality, LAI = 0.41), but a secondary layer of dense green understory (Figure 4b) yielded high green vegetation cover (97.8%) from a satellite point of view (Figure 4c; $r = 0.70$ and $p < 0.001$ after the exclusion of the outlier). Understory shrubs could potentially influence other sites as well with low LAI and high green vegetation cover. However, the impact on the linear trend was indistinguishable using the Theil–Sen estimator ($r = 0.71$, $\tau = 0.42$, and $p < 0.001$). A strong positive correlation (both parametric and nonparametric) was also found between canopy mortality and brown vegetation cover ($r \ge 0.66$, $p < 0.001$, and $n = 60$; Figure 4c), although sites with substantial fallen logs present departed slightly from the trend line (e.g., Figure 4b). Significant correlations suggest reasonably strong connections between satellite and ground measures of greenness (green canopy) and dead branches/stems (tree mortality) and indicate that the use of satellite-derived green and brown vegetation cover for regional scale analysis is reasonable.

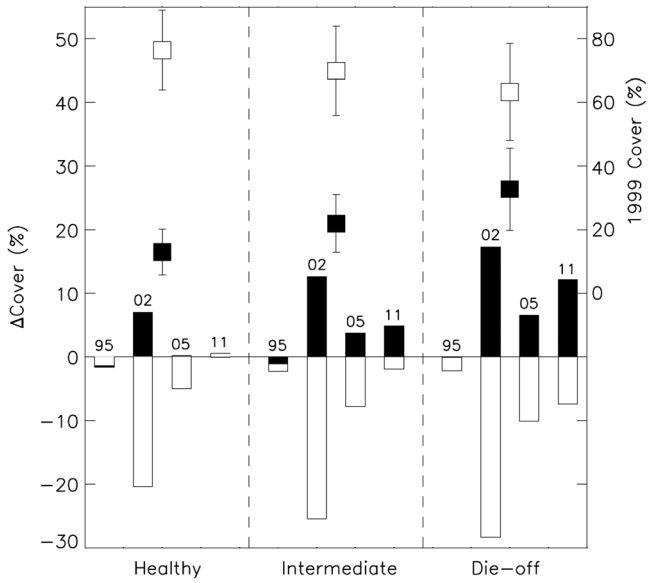

Figure 5. Temporal dynamics (years indicated by numbers) of mean differences (Δ, the left *y* axis) of green (white bars) and brown (black bars) vegetation cover fractions to those of the base year (1999) for the Healthy, Intermediate, and Die-off groups (Figure 1a). White and black boxes indicate that the mean green and brown vegetation cover fractions (the right *y* axis), respectively, of the base year and error bars depict 1 standard deviation from the mean.

3.2. Satellite Vegetation Cover

The predrought and postdrought vegetation dynamics of the aspen forests are illustrated in Figure 5. The mean (±sd) predrought (1999) green vegetation cover for the Healthy, Intermediate, and Die-off groups were 76.4 ± 12.5%, 70.0 ± 14.0%, and 63.3 ± 15.2%, respectively; the difference among the groups was statistically significant (based upon $\alpha = 0.01$ criterion via the Tukey–Kramer multiple comparison, $n = 400$ for each group). The mean predrought brown vegetation cover values were 13.0 ± 7.1% (Healthy), 21.9 ± 9.1% (Intermediate), and 32.8 ± 12.9% (Die-off), and the difference was significant as well. The mean abundances (%) of green and brown vegetation cover was quite stable (deviation ≤2.3%) before the 2002 drought by comparing 1999 values with those in 1995.

In 2002 during the drought, the mean green vegetation cover dropped significantly (Δgreen vegetation cover for the Healthy group = −20.4%, Intermediate = −25.5%, and Die-off = −28.3%), and the mean brown vegetation cover increased across all groups, with the strongest increase in brown vegetation cover occurring in areas that would later succumb to aspen die-off (Δbrown vegetation cover for the Healthy group = 7.0%, Intermediate = 12.6%, and Die-off = 17.3%).

Examining the vegetation recovery with the 2005 and 2011 vegetation cover, the green vegetation cover rebounded gradually (~3% year^{-1}) from the 2001–2003 drought for all groups (Figure 5). For the Healthy group, the mean brown vegetation cover returned to the predrought condition soon after the drought regardless of the annual precipitation variation (Figure 2). In contrast, a noticeable amount of the increases in brown vegetation cover (compared with 1999) remained in the Intermediate (Δbrown vegetation cover = 3.7–4.9%) and Die-off (Δbrown vegetation cover = 6.5–12.1%) sites. Moreover, there was a slight tendency of brown vegetation cover increase since 2005 for both groups (Intermediate = 0.2% year^{-1} and Die-off = 0.8% year^{-1}). The comparisons between the 2011 Landsat-derived green and brown vegetation cover with the 1999 predrought image revealed standing differences of postdrought recovery. The mean difference of green vegetation cover for the Healthy, Intermediate, and Die-off were 0.5%, −1.9%, and −7.4%, respectively. The difference was significant for Die-off regions ($p < 0.0001$, one-way ANOVA, $n = 800$) but not for Healthy or Intermediate areas ($p \geq 0.15$). This indicates reasonable recovery of green vegetation cover in the Healthy and Intermediate categories but not Die-off areas. Changes in brown vegetation cover between 1999 and 2011 were −0.1%, 4.9%, and 12.1% for the three categories, respectively, significant at $p < 0.0001$ for the Intermediate and Die-off categories but not for Healthy areas ($p = 0.91$).

3.3. Surface Brightness and Land Surface Temperature

The mean total shortwave albedo (±sd) was quite similar (Healthy = 12.7 ± 1.7%, Intermediate = 13.0 ± 1.8%, and Die-off = 13.7 ± 1.7%) before drought (1999) among the three groups ($n = 400$ for each group) and confirmed by the Tukey–Kramer multiple comparison procedure ($\alpha = 0.01$). The baseline condition was also very similar to the 1995 image (differences < 1%). About 13% of the brightness increase occurred in all three groups during the driest year (2002). However, the brightness differences for all groups were negligible after nearly a decade of recovery by comparing samples extracted from 2011 and 1999 Landsat images ($p > 0.11$, one-way ANOVA, $n = 400$ for each year/group).

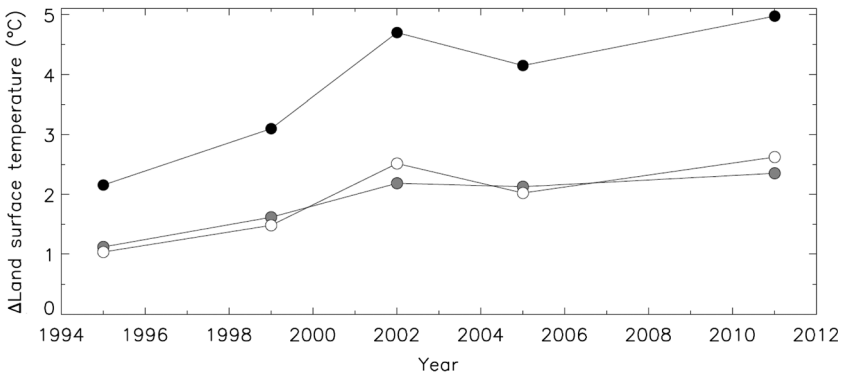

Figure 6. The differences (Δ) of mean daytime (~10:30 A.M. local time) land surface temperature during 1995–2011 between Die-off and Healthy (Die-off–Healthy) (black dots) and Intermediate (Die-off–Intermediate) (gray dots) groups, respectively, and between Intermediate and Healthy (Intermediate–Healthy) (white dots) groups.

Differences of land surface temperature among Healthy, Intermediate, and Die-off pixels existed prior to the drought with Die-off sites occupying hotter locations than Intermediate (1.0 K Δland surface temperature$_{(Die\text{-}off\text{-}Intermediate)}$) or Healthy sites (3.1 K Δland surface temperature$_{(Die\text{-}off\text{-}Healthy)}$) based on the 1995 and 1999 Landsat images, respectively (Figure 6). The differences increased during the 2002 drought period (from 2.2 K (Δland surface temperature$_{(Intermediate\text{-}Healthy)}$) to 4.7 K (Δland surface temperature$_{(Die\text{-}off\text{-}Healthy)}$)) and remained at these higher levels after the drought with the maximum Δland surface temperature$_{(Die\text{-}off\text{-}Healthy)}$ of 5.0 K in 2011 (Figure 6). The total increase in land surface temperature differences was ≥45% based on dividing Δland surface temperature acquired in 2011 by the value in 1999.

4. Discussion

Monitoring the trajectories of ecosystem responses to extreme events like drought is critical since widespread tree die-off events could potentially result in severe consequences for the biosphere in the coming decades [*Kurz et al*., 2008; *Anderegg et al*., 2012a]. Limitations in time series plot data currently limit the potential to assess the recovery of forest ecosystems at the species level, but we demonstrate here that remotely sensed monitoring of temporal vegetation, brightness, and land surface temperature dynamics makes it feasible to investigate biophysical recovery at the regional scale.

4.1. Drought and Postdrought Vegetation Cover Dynamics

Aspen is the most widely distributed tree species in North America [*Perala*, 1990] and a dominant one in some western regions [*Worrall et al*., 2010; *Michaelian et al*., 2011]. Thus, drought-induced die-off could conceivably lead to substantial carbon sources in North American temperate and boreal forest ecosystems [*Peng et al*., 2011; *Anderegg et al*., 2012a]. While aerial surveys estimate that aspen die-off conservatively affected ~17% of Colorado aspen forests [*Worrall et al*., 2010], the full distribution of recent aspen die-off across North America is not well known but appears to affect from Arizona to Alberta [e.g., *Michaelian et al*., 2011].

Significant deviations of the green and brown vegetation cover from the baseline condition were detected by satellites in the driest year (2002) for all groups (Figure 5). The variations likely reflect both initial tree mortality and plant physiological adjustments to drought through changes in leaf area or leaf shedding, since the levels of green and brown vegetation cover have returned to the predrought condition in the Healthy sites. These observed changes during the 2002 severe drought, particularly the ability to discriminate in this image between regions that would recover (Healthy/Intermediate) and regions that would later dieback (Die-off), could potentially provide a useful tool for the monitoring of drought impacts on aspen forests and early warning signs of die-off. This is especially relevant given the recurrence of a severe climate-change-type drought that happened (is happening) in 2012–2013 in the region and that ecophysiological work in these forests has suggested that surviving forests may be increasingly vulnerable to drought due to accumulated hydraulic damage [*Anderegg et al*., 2013]. In summer 2012, an ongoing research project was established to monitor potential future aspen die-off sites in the San Juan National Forest. Potential die-off sites were identified by utilizing the transient green and brown vegetation cover

changes during the 2002 drought elucidated here on an ETM+ satellite image acquired on 11 July 2012. If successful, these sites could allow monitoring of plant physiological mechanisms during and after a tree mortality event. If remote sensing analyses can provide indications of where to study in near real time with possible rapid qualitative screening using Google Earth™ high spatial resolution images (Figure 1c), this information could be incredibly valuable to elucidating the physiological mechanisms of drought-induced tree mortality in future droughts and useful as well for land managers.

The Intermediate category of forests experienced some gradual recovery of green vegetation cover through time since the 2001–2003 drought (Figure 5), but high brown vegetation cover still remained in these sites implying the existence of standing litter (tree snags) and fallen logs (Figures 1c and 1e). This is expected since it would take more than a decade for most of the carbon in coarse woody debris to be respired into the atmosphere during decomposition [*Alban and Pastor*, 1993; *Brais et al*., 2006]. In aspen die-off forests, high levels of green vegetation cover decline and brown vegetation cover increases in 2005 and 2011 from the predrought condition (even with the offset of understory shrub green cover through the gap of top layer damaged aspen trees; Figures 1e and 4b) in severely damaged Die-off sites suggest little sign of vegetation recovery in dying regions [*Anderegg et al*., 2012c]. Combining the results of this study and of our recent work [*Huang and Anderegg*, 2012], we conclude that the vegetation structure of 26.9% (or 255.6 km^2) of the aspen forests assessed (conservative estimate of Die-off sites only) may have been transformed (significant change of the green and brown vegetation cover) at least temporarily. Green vegetation cover is directly related to gap fraction and possibly LAI [*Campbell and Norman*, 1998], and thus, the loss of green cover has resulted in the degradation of these forests' productivity and transpiration of water [*Anderegg et al*., 2014]. Brown vegetation cover is a useful tool for understanding carbon cycling components such as turnover rate, fuel load, and plant stress [*Okin*, 2010]. Therefore, our results suggest that drought-induced die-off may have influenced ecosystem metabolism of regions of aspen forests for nearly a decade.

Forest die-off research often aims to understand the relationship between tree mortality and stand characteristics such as tree size (presumably related to age) and density, which is useful for prediction of future stand structure trajectories. For example, studies indicated that drought-induced tree mortality was more likely to occur in larger trees in pinyon-juniper woodlands [*Floyd et al*., 2009] and lodgepole pine forests [*Pfeifer et al*., 2011], but mortality was more likely in smaller trees in some boreal forests in Canada [*Ma et al*., 2012]. In our study region [*Anderegg et al*., 2012b] and many other cases [*van Mantgem et al*., 2009], mortality was pervasive across all stand ages. We found however an apparent relationship between predrought vegetation cover and mortality. Areas with lower green vegetation and higher brown vegetation cover before drought were more likely to suffer high tree mortality following drought (Figure 5). *Huang and Anderegg* [2012] found that tree mortality sites were commonly located on south facing slopes, which are generally drier and warmer than other landscape positions in northern hemisphere. Thus, we conclude that settings with harsh physical conditions would limit aspen tree growth, leading to more sparse and open canopies that would maintain lower green vegetation and higher brown vegetation cover and appear to have been more susceptible to drought. Indeed, spatial patterns of where aspen stands died versus survived are likely influenced by a complex set of genetic, ontogenetic, tree allocation (e.g., root-to-leaf ratio), edaphic, and climatic factors. Nonetheless, topographic factors that lead to hotter and drier sites (south facing slopes, lower elevations, and shoulder slopes [*Worrall et al*., 2008, 2010]) seem to be the dominant explanation of spatial patterns of aspen die-off. Our finding that low green vegetation cover sites generally suffered higher levels of aspen mortality also agrees with measurements of stand density, where lower predrought densities experienced higher mortality [*Worrall et al*., 2010].

4.2. Surface Brightness Dynamics and Land Surface Temperature Deviation

According to spectral reflectance values of green and brown vegetation cover of the region [*Huang and Anderegg*, 2012], the total shortwave albedo of green vegetation cover is 6.3% (up to 17.1%) lower than that of brown vegetation cover for aspen vegetation. Increases in brown vegetation cover in forest ecosystems, accompanied by a decrease of green vegetation cover, alter land surface energy budgets and can reduce the biophysical cooling effect, resulting in elevated regional temperatures [*Anderson et al*., 2011]. Massive tree mortality is generally expected to brighten surface reflectivity (Figure 1d); the loss of top layer green canopies allows sunlight passing through and can alter ecosystem energy budgets substantially [*Royer et al*., 2011]. Yet we do not find such increases in surface reflectivity. Postdrought stability of total shortwave albedo in this

region could be caused by complex biophysical interaction related to the composition of multilayer plant communities. One possible factor might be the greenness compensation from understory shrub from a satellite point of view (Figures 1e and 4b). Unlike a spectral mixture analysis that can provide subpixel information of fractions of green and brown vegetation and bare soil, calculation of brightness from Landsat images yields a single reflective value per pixel (although green vegetation cover might still be partially affected by understory; Figure 4a). Therefore, surface brightness may be insensitive to vegetation cover dynamics from above by satellite. We note that our findings do not suggest that the ramifications of die-off to aspen ecosystem functions (e.g., productivity and surface-atmosphere interaction) are minimal but imply the constraint of two-dimensional optical remote sensing and insensitivity of derived total shortwave albedo to study an ecosystem with multilayers of canopies. This constraint would likely operate in other multilayer canopy forests as well, such as tropical rainforests [e.g., *Phillips et al*. [2009]].

Our land surface temperature time series pattern reveals the apparent increase of differences among the Healthy, Intermediate, and Die-off groups beginning during drought and persisting through 2011 (Figure 6). This may be due to reduced plant transpiration in these deciduous broadleaf forests with high canopy conductance and evaporative fraction [*Breuer et al*., 2003]. We find that canopy mortality is associated with a decrease in this cooling effect, leading to larger temperature contrasts between healthy and dying regions. Previous studies also indicated that drought can modify forest canopy structure and biophysical parameters, such as the decrease of surface roughness, which may repartition the exchange of heat toward more sensible (less latent) heat transfer and alter local temperatures [*Bonan*, 1997].

5. Conclusions

The effects of extreme climatic events on forest ecosystem biophysical attributes, particularly in the temporal dynamics of drought-triggered forest die-off and recovery, are a major uncertainty in the feedback of terrestrial ecosystems on climate change. We studied the regional biophysical characteristics of aspen forests in southwestern Colorado, which experienced severe drought-induced forest mortality, by utilizing remotely sensed time series vegetation cover, surface brightness (total shortwave albedo), and land surface temperature data. Based upon the temporal dynamics of these primary land surface parameters, we conclude that large areas of these forests may have not returned to the predrought conditions after nearly a decade of recovery. Our results show that drought-induced tree mortality has altered biophysical characteristics of these aspen forests in this region, thereby affecting regional biogeochemical, hydrological, and energy cycles. We also find that the temporal dynamics of remotely sensed vegetation cover during drought itself could be a metric for assessing propensity of subsequent mortality, allowing effective regional monitoring of forest die-off and recovery and potentially providing a much-needed early warning of drought-driven tree mortality.

Acknowledgments

We appreciate the efforts of the editorial team that handled this manuscript and the four anonymous reviewers that provided constructive comments on earlier versions of the manuscript. The data for this paper are all available to anyone upon request (C.Y.H., choying@ntu.edu.tw). C.Y.H. was supported by the National Science Council (NSC) of Taiwan (NSC 98-2221-E-002-198-) and National Taiwan University (102R7604-2). We thank L. Anderegg, K. Pham, A. Nees, D. Karp, and C. Sherman for their assistance with fieldwork and providing field data. W.R.L.A. thanks Bill Lane Center for the American West, Morrison Institute of Population and Resource Studies, Phi Beta Kappa Northern California Association, Stanford Biology SCORE Program, and the NSF DDIG Program for research funding. W.R.L.A. was supported in part by an award from the NOAA Climate and Global Change Postdoctoral Fellowship.

References

ACORN (2008), *ACORN 6 User's Manual*, ImSpec LLC, Palmdale, Calif.

Alban, D. H., and J. Pastor (1993), Decomposition of aspen, spruce, and pine boles on two sites in Minnesota, *Can. J. For. Res.*, *23*, 1744–1749.

Allen, C. D., et al. (2010), A global overview of drought and heat-induced tree mortality reveals emerging climate change risks for forests, *For. Ecol. Manage.*, *259*, 660–684.

Anderegg, W. L., L. L. Anderegg, J. Berry, and C. Field (2014), Loss of whole-tree hydraulic conductance during severe drought and multi-year forest die-off, *Oecologia*, *175*, 1–13.

Anderegg, W. R. L., J. M. Kane, and L. D. L. Anderegg (2012a), Consequences of widespread tree mortality triggered by drought and temperature stress, *Nat. Clim. Change*, *3*, 30–36.

Anderegg, W. R. L., J. A. Berry, D. D. Smith, J. S. Sperry, L. D. L. Anderegg, and C. B. Field (2012b), The roles of hydraulic and carbon stress in a widespread climate-induced forest die-off, *Proc. Natl. Acad. Sci. U.S.A.*, *109*, 233–237.

Anderegg, W. R. L., L. D. L. Anderegg, C. Sherman, and D. S. Karp (2012c), Effects of widespread drought-induced aspen mortality on understory plants, *Conserv. Biol.*, *26*, 1082–1090.

Anderegg, W. R. L., L. Plavcova, L. D. L. Anderegg, U. Hacke, J. A. Berry, and C. B. Field (2013), Drought's legacy: Hydraulic deterioration underlies widespread aspen die-off and portends increased future vulnerability, *Global Change Biol.*, *19*, 1188–1196.

Anderson, R. G., et al. (2011), Biophysical considerations in forestry for climate protection, *Front. Ecol. Environ.*, *9*, 174–182.

Asner, G. P., and D. B. Lobell (2000), A biogeophysical approach for automated SWIR unmixing of soils and vegetation, *Remote Sens. Environ.*, *74*, 99–112.

Asner, G. P., D. E. Knapp, A. Balaji, and G. Paez-Acosta (2009), Automated mapping of tropical deforestation and forest degradation: CLASlite, *J. Appl. Remote Sens.*, *3*, 033,543–033,524.

Bateson, A. C., G. P. Asner, and C. A. Wessman (2000), Endmember bundles: A new approach to incorporating endmember variability into spectral mixture analysis, *IEEE Trans. Geosci. Remote Sens.*, *38*, 1083–1094.

Bonan, G. B. (1997), Effects of land use on the climate of the United States, *Clim. Change*, *37*, 449–486.

Bonan, G. B. (2008), Forests and climate change: Forcings, feedbacks, and the climate benefits of forests, *Science*, *320*, 1444–1449.

Brais, S., D. Pare, and C. Lierman (2006), Tree bole mineralization rates of four species of the Canadian eastern boreal forest: Implications for nutrient dynamics following stand-replacing disturbances, *Can. J. For. Res.*, *36*, 2331–2340.
Bréda, N. J. J. (2003), Ground-based measurements of leaf area index: A review of methods, instruments and current controversies, *J. Exp. Bot.*, *54*, 2403–2417.
Breuer, L., K. Eckhardt, and H.-G. Frede (2003), Plant parameter values for models in temperate climates, *Ecol. Model.*, *169*, 237–293.
Campbell, G. S., and J. M. Norman (1998), *An Introduction to Environmental Biophysics*, Springer-Verlag, New York.
Fernandes, R., and S. G. Leblanc (2005), Parametric (modified least squares) and non-parametric (Theil-Sen) linear regressions for predicting biophysical parameters in the presence of measurement errors, *Remote Sens. Environ.*, *95*, 303–316.
Floyd, M. L., M. Clifford, N. S. Cobb, D. Hanna, R. Delph, P. Ford, and D. Turner (2009), Relationship of stand characteristics to drought-induced mortality in three Southwestern piñon-juniper woodlands, *Ecol. Appl.*, *19*, 1223–1230.
Gower, S. T., J. G. Vogel, J. M. Norman, C. J. Kucharik, S. J. Steele, and T. K. Stow (1997), Carbon distribution and aboveground net primary production in aspen, jack pine, and black spruce stands in Saskatchewan and Manitoba, Canada, *J. Geophys. Res.*, *102*, 29,029–29,041, doi:10.1029/97JD02317.
Hanna, P., and D. Kulakowski (2012), The influences of climate on aspen dieback, *For. Ecol. Manage.*, *274*, 91–98.
Harris, A. T., G. P. Asner, and M. E. Miller (2003), Changes in vegetation structure after long-term grazing in pinyon-juniper ecosystems: Integrating imaging spectroscopy and field studies, *Ecosystems*, *6*, 368–383.
Hicke, J. A., et al. (2012), Effects of biotic disturbances on forest carbon cycling in the United States and Canada, *Global Change Biol.*, *18*, 7–34.
Hogg, E. H., J. P. Brandt, and M. Michaelian (2008), Impacts of a regional drought on the productivity, dieback, and biomass of western Canadian aspen forests, *Can. J. For. Res.*, *38*, 1373–1384.
Huang, C., and W. R. L. Anderegg (2012), Large drought-induced aboveground live biomass losses in southern Rocky Mountain aspen forests, *Global Change Biol.*, *18*, 1016–1027.
Huang, C., G. P. Asner, R. Martin, N. Barger, and J. Neff (2009), Multiscale analysis of tree cover and aboveground carbon stocks in pinyon-juniper woodlands, *Ecol. Appl.*, *19*, 668–681.
Huang, C., G. P. Asner, N. Barger, J. Neff, and L. Floyd-Hanna (2010), Regional carbon losses due to drought-induced tree dieback in piñon-juniper ecosystems, *Remote Sens. Environ.*, *114*, 1471–1479.
Isaaks, E. H., and R. M. Srivastava (1989), *Applied Geostatistics*, Oxford Univ. Press, New York.
Jelaska, S. D., O. Antonić, M. Božić, J. Križan, and V. Kušan (2006), Responses of forest herbs to available understory light measured with hemispherical photographs in silver fir-beech forest in Croatia, *Ecol. Model.*, *194*, 209–218.
Keen, R. A. (1996), Weather and climate, in *The Western San Juan Mountains: Their Geology, Ecology, and Human History*, edited by R. Blair, pp. 113–126, Univ. of Colorado Press, Boulder, Colo.
Kurz, W. A., C. C. Dymond, G. Stinson, G. J. Rampley, E. T. Neilson, A. L. Carroll, T. Ebata, and L. Safranyik (2008), Mountain pine beetle and forest carbon feedback to climate change, *Nature*, *452*, 987–990.
Liang, S. (2000), Narrowband to broadband conversions of land surface albedo I: Algorithms, *Remote Sens. Environ.*, *76*, 213–238.
Lowry, J., et al. (2007), Mapping moderate-scale land-cover over very large geographic areas within a collaborative framework: A case study of the Southwest Regional Gap Analysis Project (SWReGAP), *Remote Sens. Environ.*, *108*, 59–73.
Ma, Z., C. Peng, Q. Zhu, H. Chen, G. Yu, W. Li, X. Zhou, W. Wang, and W. Zhang (2012), Regional drought-induced reduction in the biomass carbon sink of Canada's boreal forests, *Proc. Natl. Acad. Sci. U.S.A.*, *109*, 2423–2427.
McDowell, N. G., D. J. Beerling, D. D. Breshears, R. A. Fisher, K. F. Raffa, and M. Stitt (2011), The interdependence of mechanisms underlying climate-driven vegetation mortality, *Trends Ecol. Evol.*, *26*, 523–532.
Michaelian, M., E. H. Hogg, R. J. Hall, and E. Arsenault (2011), Massive mortality of aspen following severe drought along the southern edge of the Canadian boreal forest, *Global Change Biol.*, *17*, 2084–2094.
Mitton, J. B., and M. C. Grant (1996), Genetic variation and the natural history of quaking aspen, *BioScience*, *46*, 25–31.
Okin, G. S. (2010), The contribution of brown vegetation to vegetation dynamics, *Ecology*, *91*, 743–755.
Pastor, J., J. D. Aber, and J. M. Melillo (1984), Biomass prediction using generalized allometric regressions for some northeast tree species, *For. Ecol. Manage.*, *7*, 265–274.
Peng, C., Z. Ma, X. Lei, Q. Zhu, H. Chen, W. Wang, S. Liu, W. Li, X. Fang, and X. Zhou (2011), A drought-induced pervasive increase in tree mortality across Canada's boreal forests, *Nat. Clim. Change*, *1*, 467–471.
Perala, D. A. (1990), Populus tremuloides, in *Silvics of North America. Hardwoods*, edited by R. M. Burns and B. H. Honkala, pp. 555–569, US Department of Agriculture, Washington, D. C.
Pfeifer, E. M., J. A. Hicke, and A. J. H. Meddens (2011), Observations and modeling of aboveground tree carbon stocks and fluxes following a bark beetle outbreak in the western United States, *Global Change Biol.*, *17*, 339–350.
Phillips, O. L., et al. (2009), Drought sensitivity of the Amazon rainforest, *Science*, *323*, 1344–1347.
Ramsey, F. L., and D. W. Schafer (1997), *The Statistical Sleuth: A Course in Methods of Data Analysis*, Duxbury Press, Pacific Grove, Calif.
Royer, P. D., N. S. Cobb, M. J. Clifford, C. Huang, D. D. Breshears, H. D. Adams, and J. C. Villegas (2011), Extreme climatic event-triggered overstorey vegetation loss increases understorey solar input regionally: Primary and secondary ecological implications, *J. Ecol.*, *99*, 714–723.
Ryu, Y., T. Nilson, H. Kobayashi, O. Sonnentag, B. E. Law, and D. D. Baldocchi (2010), On the correct estimation of effective leaf area index: Does it reveal information on clumping effects?, *Agric. For. Meteorol.*, *150*, 463–472.
van Mantgem, P. J., et al. (2009), Widespread increase of tree mortality rates in the Western United States, *Science*, *323*, 521–524.
Welles, J. M., and S. Cohen (1996), Canopy structure measurement by gap fraction analysis using commercial instrumentation, *J. Exp. Bot.*, *47*, 1335–1342.
Worrall, J. J., L. Egeland, T. Eager, R. A. Mask, E. W. Johnson, P. A. Kemp, and W. D. Shepperd (2008), Rapid mortality of *Populus tremuloides* in southwestern Colorado, USA, *For. Ecol. Manage.*, *255*, 686–696.
Worrall, J. J., S. B. Marchetti, L. Egeland, R. A. Mask, T. Eager, and B. Howell (2010), Effects and etiology of sudden aspen decline in southwestern Colorado, USA, *For. Ecol. Manage.*, *260*, 638–648.
Worrall, J. J., G. E. Rehfeldt, A. Hamann, E. H. Hogg, S. B. Marchetti, M. Michaelian, and L. K. Gray (2013), Recent declines of *Populus tremuloides* in North America linked to climate, *For. Ecol. Manage.*, *299*, 35–51.
Yamane, T. (1967), *Statistics: An Introductory Analysis*, Harper and Row, New York.
Zhang, Y., J. M. Chen, and J. Miller (2005), Determining exposure of digital hemispherical photographs for leaf area index estimation, *Agric. For. Meteorol.*, *133*, 166–181.